ACS APPLIED MATERIALS & INTERFACES

Research Article

www.acsami.org

# In Situ Mapping of the Molecular Arrangement of Amphiphilic Dye Molecules at the $TiO_2$ Surface of Dye-Sensitized Solar Cells

Kislon Voïtchovsky,[†,‡,#] Negar Ashari-Astani,[§,#] Ivano Tavernelli,[§,⊥] Nicolas Tétreault,[∥] Ursula Rothlisberger,[§] Francesco Stellacci,[†] Michael Grätzel,[∥] and Hauke A. Harms*[,∥]

[†]EPFL STI IMX SUNMIL, Station 12, CH-1015 Lausanne, Switzerland

[‡]Physics Department, Durham University, Durham DH1 3LE, United Kingdom

[§]EPFL SB ISIC LCBC, BC, CH-1015 Lausanne, Switzerland

[∥]EPFL SB ISIC LPI, Station 6, CH-1015 Lausanne, Switzerland

Supporting Information

**ABSTRACT:** Amphiphilic sensitizers are central to the function of dye-sensitized solar cells. It is known that the cell's performance depends on the molecular arrangement and the density of the dye on the semiconductor surface, but a molecular-level picture of the cell−electrolyte interface is still lacking. Here, we present subnanometer in situ atomic force microscopy images of the Z907 dye at the surface of $TiO_2$ in a relevant liquid. Our results reveal changes in the conformation and the lateral arrangement of the dye molecules, depending on their average packing density on the surface. Complementary quantitative measurements on the ensemble of the film are obtained by the quartz-crystal microbalance with dissipation technique. An atomistic picture of the dye coverage-dependent packing, the effectiveness of the hydrophobic alkyl chains as blocking layer, and the solvent accessibility is obtained from molecular dynamics simulations.

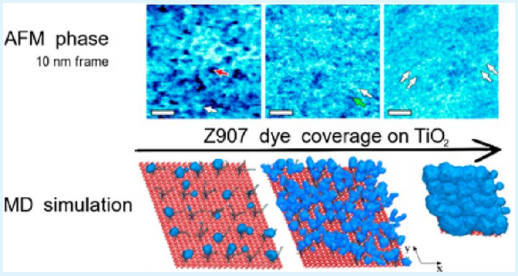


**KEYWORDS:** *atomic force microscopy, dye-sensitized solar cells, Z907, molecular dynamics simulations, liquid phase*

## 1. INTRODUCTION

Surface functionalization with self-assembled monolayers (SAMs) is of fundamental importance to nanotechnology, with applications ranging from molecular electronics to controlled wetting, sensing, medical devices, and energy harvesting systems.[1−5] SAM functionalization provides a powerful, yet simple way to manipulate the chemical, electrical, and optical properties of surfaces, with the ability to tune the material's macroscopic properties.[6] This is the case for dye-sensitized solar cells (DSCs) where a SAM of dye molecules sensitizes a semiconductor in order to harvest light. DSCs provide a viable alternative to traditional semiconductor solar cells due to their high efficiency and low environmental and industrial costs.[5,7−11] The heart of the DSC is composed of the dye SAM adsorbed on a wide-bandgap semiconductor, usually a high surface area mesoporous $TiO_2$ photoanode, infiltrated with an electrolyte containing the redox shuttle molecule. The primary role of the dye SAM is to sensitize the $TiO_2$ semiconductor, similar to sensitization of silver halides in paper photography. Upon illumination, the dye goes into a photoexcited state and can inject an electron into the conduction band of the semiconductor. The oxidized dye is regenerated by a hole conductor, traditionally a liquid electrolyte, covering the dye and containing a redox mediator. The molecular dye film has also a secondary function: it must act as an electronic barrier that prevents the photoinjected electrons to recombine with the oxidized form of the redox mediator present in the electrolyte. For typical dye molecules, this is ensured by hydrophobic alkyl chains that hinder the redox-mediator from accessing the semiconductor surface, and prevent lateral aggregation of dye molecules. The anchoring groups of the dye, usually carboxylic acids, are hydrophilic, which gives the dye an amphiphilic character and behavior often similar to anionic surfactants. The DSC macroscopic efficiency is known to depend on both the molecular arrangement of the adsorbed dye layer and the contacting electrolyte. This is generally true for most SAM-functionalized surfaces, which requires linking in situ molecular-level details with macroscopic observations in order to derive a full understanding.[12]

Practically, gaining in situ information about the molecular arrangement of dye-sensitizers often proves challenging. Fourier transform infrared spectroscopy was successfully used to observe the binding of dye molecules to the $TiO_2$ surface of DSCs.[9,13] The average orientation of adsorbed molecules relative to the surface could be derived from combined near-edge X-ray absorption fine structure spectroscopy (NEXAFS) and photoelectron spectroscopy (PES).[14−16] However, the irregular mesoporous titania surface prevents averaging techniques from capturing local molecular details. Scanning

Received: March 2, 2015
Accepted: May 4, 2015
Published: May 4, 2015







DOI: 10.1021/acsami.5b01638
ACS Appl. Mater. Interfaces 2015, 7, 10834−10842

probe techniques can, in principle, overcome this difficulty and provide direct, local information about the adsorbed layer. Scanning tunneling microscopy studies in ultrahigh vacuum achieved the first submolecular resolution images of the dye layer, but the measurements were conducted far from the functional conditions of a DSC.[17,18] Ex situ atomic force microscopy (AFM) results indicated the existence of large dye aggregates on the flat $TiO_2$ substrate for standard device preparation procedure, but molecular resolution was not achieved.[19]

Recent developments in the field of AFM have made it possible to achieve subnanometer mapping of soft and hard surfaces in solution paving the way for in situ local observations of a functional DSC surface.[20−22]

Here, we report in situ molecular-level AFM images of adsorbed dye molecules at mesoporous and flat $TiO_2$ surfaces in a device-relevant liquid. We used the amphiphilic ruthenium complex Z907 (diphenyl-nonyl diphenyl-carboxyl dithio octaruthenium) dye (insert in Figure 2) due to its widespread use in DSCs, its good performance in long-term stability tests, and the fact that it is less prone to aggregation than other dyes.[23,24] The AFM study is conducted with the sample fully immersed either in ethyl-isoproyl sulfone (EiPS), or acetonitrile (MeCN), both solvents being used for electrolytes in functional DSCs. We show that under normal conditions, the dye forms a single monolayer over the surface. The molecular conformation of the dye depends on the density coverage with domains of different molecular conformation able to coexist within the adsorbed submonolayer. The AFM results are complemented with measurements conducted using the quartz crystal microbalance with dissipation technique (QCM-D) so as to assess the average quantity of adsorbed molecules on the substrate with respect to coverage saturation. The experimental AFM and QCM-D results are supported by molecular dynamics (MD) simulations of dyes adsorbed on the (101) facet of anatase $TiO_2$ immersed in acetonitrile solvent.[25−27] The simulations provide atomic-level insight into the density-dependent changes in the arrangement of the adsorbed Z907 molecules.

## 2. METHODS

**2.1. AFM.** The AFM data were acquired on a commercial Multimode Nanoscope IIIa (Digital Instruments, now Bruker, Santa Barbara, CA) operated in amplitude-modulation. The sample and the scanning tip were fully immersed into the imaging liquid (EiPS or MeCN, respectively). Before each experiment, the liquid cell was thoroughly washed in isopropanol and ultrapure water and subsequently dried with nitrogen. We used standard silicon nitride cantilevers (Olympus RC800 PSA, Olympus, Tokyo) with a nominal stiffness of $k_n$ = 0.76 N/m. In each experiment, the cantilever was driven acoustically with the liquid cell, close to its resonance frequency. Typical imaging amplitudes $A$ were kept between 0.5 and 1.5 nm with the set point ratio $A/A_0$ as large as possible ($A_0$ is the free vibration amplitude in liquid). The use of relatively soft cantilevers and working amplitudes commensurate with the thickness of the sample−liquid interface allow us to exploit short-range solvation forces so as to enhance the resolution. In these particular imaging conditions, the energy dissipated by the vibrating AFM tip is not sufficient to fully remove the liquid between the tip and the sample, and the tip mainly probes the properties of the interfacial liquid at the surface of the sample.[12,22,28] The phase contrast is then related to the local wetting properties of the sample, that is, the local solvation free energy[12,22] or, at the macroscopic level, the solid−liquid work of adhesion. In practice, imaging over the $TiO_2$ substrate provides a darker phase contrast than over the Z907 regions, indicating a higher affinity of the solvent for the substrate than for the dye-covered surface (Figure 3c). If larger imaging amplitudes are used, the phase contrast then reflects mainly the mechanical properties of the sample, but working at large amplitudes is generally detrimental for resolution.[28]

**2.2. QCM-D.** The quartz microbalance with dissipation technique (QCM-D) directly measures mass uptake on a sensor crystal inside a flow cell. It also allows for simultaneous detection of the viscoelastic properties of the adsorbed molecular layer. In the Q-Sense E4 instrument we are using, the quartz crystal sensor is contacted by gold electrodes, and its sensing side is coated with 67 nm of $TiO_2$ by the same atomic layer deposition (ALD) process that is used for coating the silicon substrates used for AFM measurements. The sensor is placed into a flow cell where its $TiO_2$ side can be exposed to liquid dye solution in order to measure mass change in situ. Given the molecular weight of the Z907 dye molecule, the QCM-D technique is sensitive enough to quantify submonolayers of adsorbed molecules on flat $TiO_2$ film; see Harms et al.[27] for details.

**2.3. Computational Methods.** Classical MD simulations were performed for different dye coverage and various packing modes and molecular orientations. The $TiO_2$ surface was described by the Bandura Kubicki force field, whereas for the Z907 dye, a force field was developed following the AMBER protocol.[29−31] Classical point charges were derived using the RESP procedure except for the carboxylic anchoring groups whose charges were chosen in such a way as to reproduce the experimental adsorption energy.[32,33] For this purpose we used the Gaussian 09 Package.[34] The force field was validated via full ab initio simulations of a single dye in vacuum. A united atom optimized potentials for liquid simulations (OPLS) force field was employed for acetonitrile.[35]

Experimental and computational studies have suggested different binding modes for Z907 and similar dyes.[9,36−38] Initial tests showed that the different binding modes (dissociative, bidentate, or monodentate) hardly affect the space occupied by each dye and hence have little influence on the overall packing geometries. For all studies presented here, we thus have adopted a single, nondissociative bidendate binding mode.

Initial models of the system composed of two layers of anatase $TiO_2$ (108 × 113 Å$^2$ for low and medium coverage and 54 × 56 Å$^2$ for high coverage) were constructed using Materials Studio.[39] Molecular dynamics simulations were performed with the Amber 12 package using the PMEMD module.[29]

Production runs of about 20 ns in the NVE ensemble were sampled after initial minimization and 5 ns of equilibration in the canonical ensemble using Nosé−Hoover thermostats at room temperature (300 K).

**2.4. Sample Preparation.** $TiO_2$ samples for AFM measurements were based on a (100) silicon wafer substrate coated with titanium dioxide by atomic layer deposition from a tetrakis (dimethylamino) titanium (TDMAT) precursor, as described previously.[40] The $TiO_2$ film of 67 nm thickness was annealed at 420 °C and had a surface roughness of ∼2.0 nm on a 4 $\mu$m AFM frame. X-ray diffraction of the film showed evidence of anatase crystallites but no rutile phase (Supporting Information). The Z907 pigment was dissolved in a 1:1 volumetric mixture of *tert*-butanol and acetonitrile, and a solution of 50.0 $\mu$M concentration was quantified by an absorption measurement using the published extinction coefficient of 12 200 M$^{-1}$ cm$^{-1}$; lower concentrations were obtained by dilution.[23]

Prior to staining, the AFM substrates were cleaned by UV−ozone for 10 min and subsequently heated for 30 min at 420 °C to remove organic residuals and excess water from the $TiO_2$ surface. After cooling to 70 °C, they were immersed into the dye solution for 30 min, rinsed in $^t$BuOH:MeCN mixture, immersed in MeCN for 30 min, stained again for 10 min, rinsed in $^t$BuOH:MeCN mixture and MeCN, and subsequently stored in MeCN in the dark.

Samples destined for AFM measurements were usually transferred to EiPS as an imaging liquid. EiPS is a main constituent in nonvolatile high-voltage electrolytes that are used in industrial applications of dye-sensitized solar cells.[41,42] EiPS was chosen for its relevance in DSC applications and for its low vapor pressure (compared to MeCN), making it is easier to reach stable imaging conditions at high


DOI: 10.1021/acsami.5b01638
ACS Appl. Mater. Interfaces 2015, 7, 10834−10842

resolution. Aside from experimental considerations, no differences could be seen in the images obtained in MeCN and EiPS (Supporting Information, Figure S1).

## 3. RESULTS

Figure 1 shows a high-resolution image of the surface of a DSC in a functionally relevant liquid. The measurement, conducted

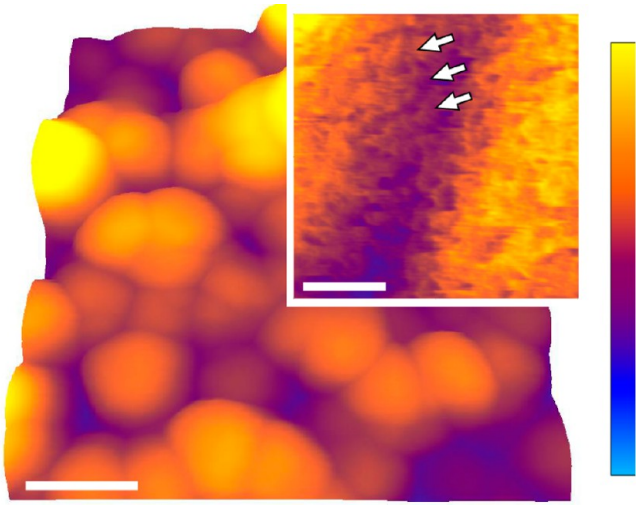

**Figure 1.** High-resolution AFM image of the surface of a DSC in liquid. The surface is composed of mesoporous $TiO_2$ stained with the Z907 ruthenium dye. The $TiO_2$ nanoparticles are clearly visible in the main image. (Inset) Molecular detail of the dye arrangement at the edge of a nanoparticle with some ordering visible (arrows). The scale bars are (main image) 40 nm and (inset) 3 nm. The color scale is (main image) 70 nm and (inset) 6 nm.

with AFM in EiPS, provides unique insight into the subnanometer details of the device's surface and indicates some structure in the dye layer. The dye molecules appear to be arranged along some preferential directions (arrows in the inset) although no long-range order is visible. However, these results should be taken cautiously due to the high surface curvature of mesoporous $TiO_2$, which renders AFM imaging challenging due to tip-convolution effects. An additional difficulty arises from the fact that dye molecules tend to accumulate primarily in holes and surface grooves at intermediate coverage, making a study of the dye molecular arrangement as a function of surface coverage difficult.

To overcome these difficulties, we have used flat $TiO_2$ substrates throughout this study. The substrates, obtained by atomic layer deposition, present a sufficiently low roughness on the nanoscale to avoid ambiguous interpretation of the AFM results. For each sample, the actual surface coverage is determined by QCM-D so as to ensure that the local AFM observations reflect global surface properties. The adsorption behavior of the same Z907−$TiO_2$ system has previously been studied by using a QCM-D.[27] Figure 2 shows the adsorption isotherm for Z907 on flat $TiO_2$ films. The figure uses previously published data[27] as a reference for comparison with the current measurements. The isotherm follows a Langmuir-type behavior (red line), indicating a saturation value of 103 ng $cm^{-2}$ area mass uptake over the concentration range on display. This corresponds to 0.76 molecules/$nm^2$, or a molecular footprint of 1.31 $nm^2$/molecule when assuming a flat surface. We define this saturation value as 100% mass coverage, which should correspond to a densely packed monolayer of Z907. For

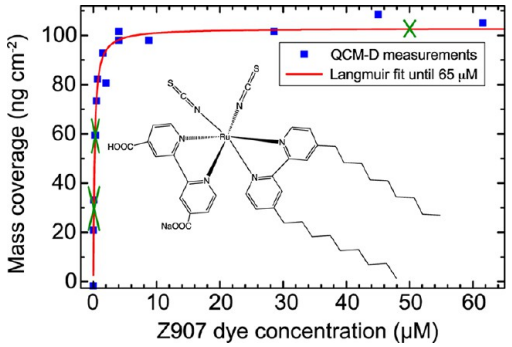


**Figure 2.** QCM-D area mass uptake over concentration of sensitizing dye solution with a Langmuir isotherm fitted to the data. Blue data points are taken from previously published experiments.[27] Green crosses mark the three concentrations of dye solutions used for staining the AFM samples and indicate their corresponding mass coverage. (Inset) Structure of the Z907 ruthenium dye.

staining the AFM samples, dye concentrations were chosen such that a mass coverage of approximately 30, 60, or 100% was obtained (green data crosses in Figure 2).

A representative AFM topographic image of the flat $TiO_2$ surface after sensitization with dye molecules (30% mass coverage) is shown in Figure 3a. The image shows large protrusions (20−30 nm wide, and ∼2 nm high) that are related to the roughness of the $TiO_2$ substrate. Details of the dye molecules are already visible, appearing as a subnanometer, mostly homogeneous roughness on the surface. This is confirmed in higher magnification images of the sample where the dye film appears as homogeneous sponge-like structure (Figure 3a, inset). Using harsh imaging conditions, it is possible to mechanically remove dye molecules in selected regions by scratching. The scratched region, which corresponds to the $TiO_2$ substrate, appears darker in the phase image (purple arrow, Figure 3b,c). This phase contrast indicates a higher affinity of the solvent for the $TiO_2$ than for the dye, and could be consistently used throughout this study to identify dye-covered (light) and uncovered (dark) regions.[12,22] At 30% mass coverage, the dye layer exhibits dark spots in the phase, suggesting that uniform gaps exist between the adsorbed Z907 molecules. These gaps give the apparent sponge-like appearance to the dye layer topography. The thickness of the dye film is difficult to evaluate directly from Figure 3a due to the roughness of the substrate. It is, however, possible to use the exposed $TiO_2$ region as a reference. A line profile taken at the edge of the dye layer indicates a thickness of ∼0.6 nm (Figure 3d). This value is a lower estimate of the real thickness due to the mechanical perturbation induced by the AFM tip on the dye molecules during the imaging process.

A closer look at Figure 3a reveals occasional variations in the height of the dye layer over flat substrate regions (blue arrows). These regions hint to local variations of the Z907 molecular arrangement on the substrate surface, which could be related to the density of dye molecules. To examine this effect in a systematical manner, we acquired high-resolution AFM images of the dye layer at different mass coverage, as determined by QCM-D.

Representative AFM images are presented in Figure 4 for 0, 30, 60, and 100% mass coverage. A clear trend is visible in both the topography and the phase with the increase of dye coverage. The bare substrate (0%) appears relatively rough, the image is noisy and provides little phase contrast. At 30% mass


DOI: 10.1021/acsami.5b01638
ACS Appl. Mater. Interfaces 2015, 7, 10834−10842

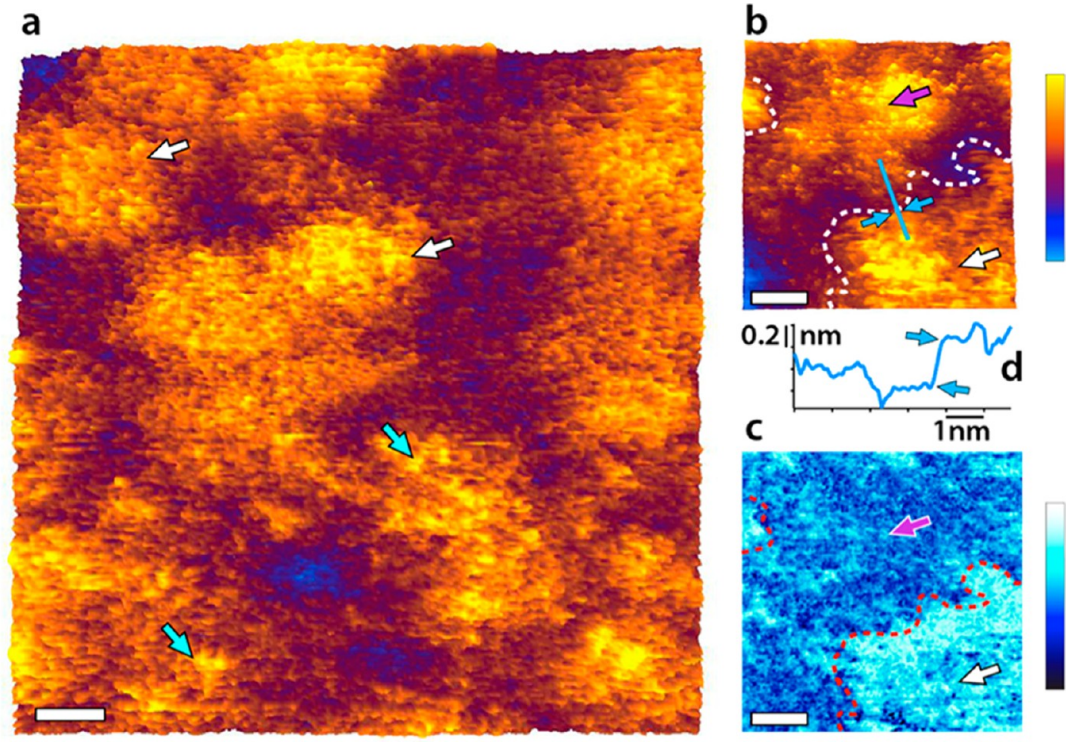


**Figure 3.** AFM micrographs of a $TiO_2$ surface covered with Z907 ruthenium dye (30% mass coverage). (a) A low-magnification (100 nm) topographic image shows almost uniform coverage by the dye apart for a few higher dye domains (blue arrows). The ~20 nm wide protrusions (white arrows) are related to the substrate roughness. Higher resolution (b) topographic and (c) phase images of the surface reveal a sponge-like structure of the dye layer (white arrow). The substrate can also be exposed by scratching with the AFM tip. The exposed $TiO_2$ substrate (purple arrow) exhibit a clear phase contrast (dotted red line) with the lighter Z907 domains. (d) Topographic profile taken over the $TiO_2$-Z907 border (blue line in panel b) indicates a thickness of ~0.6 nm for the Z907 dye layer. The topographic images are always represented with an orange−blue color scale, and the phase images in blue−black throughout the paper. Scale bars are (a) 10 nm and (b and c) 3 nm. Color bars are (a and b) 3 nm and (c) 15°.

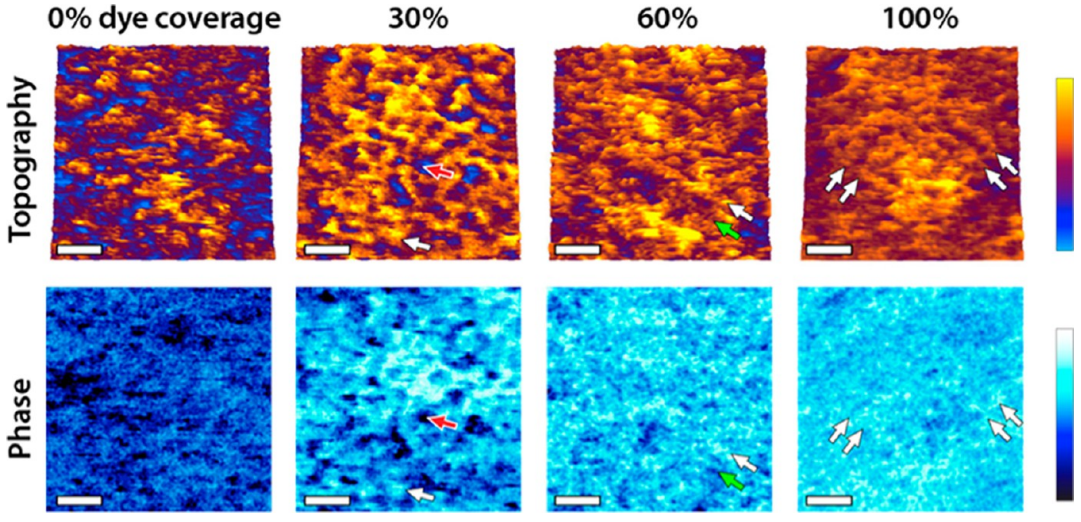


**Figure 4.** High-resolution AFM images of the dye layer at 0, 30, 60, and 100% mass coverage obtained in similar imaging conditions. At 0% the substrate appears rough and noisy due to short-range tip−sample attractive interactions. At 30%, the dye molecules (white arrow) assemble in a soft sponge-like disordered structure that can easily be disrupted by the AFM tip. Multiples holes are visible in the layer (red arrow) and appear darker in the phase. At 60%, the layer is partially ordered with the apparition of rows (white arrow) and less ordered lower regions (green arrow). At 100% the surface is fully covered, it appears smooth, and only dye rows are visible (white arrows). The scale bar is 2 nm and the color scales are 1 nm (topography) and 15° in all images.

coverage, 1−3 nm wide dye features are visible in both topography and the phase, and form a soft sponge-like layer probably templated by the atomic structure of the $TiO_2$ substrate. From the phase image, the holes (red arrow) can be attributed to the substrate, while the top of the layer is due to dye molecules and appear already more regular and smoother than bare raw substrate (white arrow). At 60% mass coverage, the layer is more ordered and appears in an


DOI: 10.1021/acsami.5b01638
ACS Appl. Mater. Interfaces 2015, 7, 10834−10842

intermediate situation where the dye molecules form both rows (white arrow) and lower, less ordered regions (green arrow). The fully covered surface appears smooth with little height variations. The whole surface is covered in row-like domains, which are not necessarily aligned (arrows). The phase image becomes consistently brighter as the surface coverage increases, indicating the substrate is fully covered at 100% mass coverage.

Interestingly, the dye molecules always spread over all the space available and never form isolated islands. At 10% mass coverage, the spreading of the dye molecules prevented nondestructive imaging (not shown).

The AFM results suggest a change in the molecular arrangement of the dye molecules on the surface as the dye coverage increases. The coexistence of two height levels at intermediate coverage supports this explanation. The formation of dye rows at higher coverage (also visible in MeCN; Figure S1, Supporting Information) is consistent with the observations on the mesoporous $TiO_2$ (Figure 1) and coincide with an increased layer thickness, suggesting that the Z907 molecules sit with their alkyl chains extended away from the substrate surface when arranged in rows (Figure 7). This interpretation would also explain the increased surface density of dye at higher mass coverage, especially given the fact that the dye molecules spread over the whole available $TiO_2$ at all coverage conditions.

To further explore the atomistic arrangement of the dye film on the $TiO_2$ surface, we performed molecular dynamics simulations at different dye densities. We simulated 100% mass coverage using a density of 0.76 molecules/nm$^2$ as obtained from QCM-D measurements. The dye molecules were arranged on a crystalline anatase (101) $TiO_2$ slab with two layers. Possible binding locations were identified based on geometric arguments: using an approximate distance between the two carboxylic groups of a bipyridine moiety of ca. 7 Å as a gauge, we tried to find adsorbing sites on the substrate with the same distance. Five possible locations were identified, as displayed in Figure 5. The same five locations were confirmed by random adsorption simulations where dyes initially located at 10−15 Å distance from the surface in vacuum were allowed to adsorb randomly during the first nanosecond of the simulation. For each of the five binding locations, a regular system of 25 dyes adsorbed on the titanium oxide surface was constructed. After minimization, the lowest energy configuration (Site 1 in Table 1) was chosen for conducting further simulations to study the effect of coverage density on packing.

As a further validation, we performed annealing simulations of all 5 systems, in which the temperature was raised to 600 K followed by cooling down to low temperatures. Consistent with the relative energetics shown in Table 1, dyes located in the energetically most stable site 1 arrangement remained at their binding sites, whereas other configurations went through several transitions between different arrangements (for configurations with sites 5, 2, and 4) and occasionally detached from the surface (in the case of site 3). An additional parameter that strongly influences the energetics of the packing is the orientation of the dye. For instance in the most stable orientation for site 1, the sulfur atoms are inversely aligned along the $[10\bar{1}]$ direction, whereas the opposite orientation is less stable (Supporting Information, Figure S2).

To visualize the effect of dye coverage on the conformation of the dye layer, we computed a topographic picture of the system comprising 25 dye molecules averaged over 20 ns of simulation (Figure 6), comparing 33% mass coverage (0.23 molecules nm$^{-2}$), 66% mass coverage (0.51 molecules nm$^{-2}$),

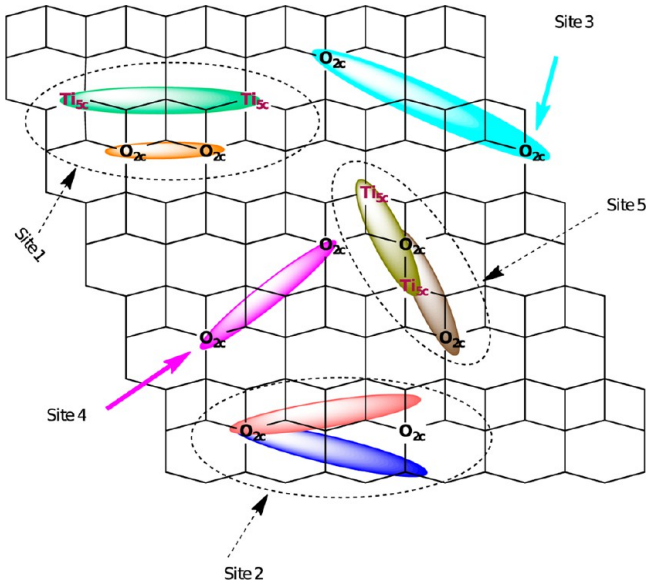


**Figure 5.** Five possible location sites suitable for simultaneous anchoring of the carboxygroups of the bipyridine moiety. The Z907 dye always occupies roughly the same (dotted) area in sites 1, 2 and 5, regardless of the selected binding mode inside the ellipse. For site 1, Z907 in its fully protonated structure can make hydrogen bonds with two 2-coordinated oxygens ($O_{2c}$). In its deprotonated state, the bipyridine moiety can make bonds to 5-coordinated Ti ($Ti_{5c}$), either way occupying the same space shown in dots. The same holds true for site 5. For site 2, the bipyridine can be in the salmon-colored ellipse or the blue one; in either, it can make hydrogen bonds to the same two ridge oxygens indicated.

**Table 1. Relative Energetics for Different Dye Location Sites[a] Evaluated for a System Composed of 25 Dyes[b]**

| adsorption site | relative energetics (kcal/mol dye molecule) |
|---|---|
| site 1 | 0 |
| site 2 | 15.4 |
| site 3 | 25.6 |
| site 4 | 30.8 |
| site 5 | 48.7 |

[a]Displayed in Figure 5. [b]The relative energetics was evaluated for a 33% mass coverage system where dye−dye interactions are less important.

and 100% mass coverage (0.76 molecules nm$^{-2}$). To change the mass coverage in the computations, we adjusted the size of the $TiO_2$ slab accordingly and kept the number of dye molecules constant. At lower densities, one of the lipophilic alkyl chains is mostly extended parallel to the surface whereas the other is pointing upward (Figure 7). This leads to a configuration where the dyes are packed closer to the surface, that is, the average layer distance is ca. 8.7 Å with an average tilting angle of 38 ± 6° of the bipyridine moiety with respect to the titanium oxide surface. Figure 7 shows that for 100% dye coverage, the atomic density profile along the $z$ direction has a shoulder around 13 Å, and the probability to find dye atoms (mostly from the alkyl chains) in this range (13−25 Å) is higher than the one of the 33% mass coverage system (Figure 7d). In fact, at higher densities (66 and 100%), both alkyl chains of each dye molecule start to be oriented vertically with respect to the $TiO_2$ surface with average dye-layer thicknesses of approximately 9.0 and 10.2 Å and an average tilting angle of 42 ± 3° and 55 ± 3°, respectively (Figure 7; note that


DOI: 10.1021/acsami.5b01638
ACS Appl. Mater. Interfaces 2015, 7, 10834−10842

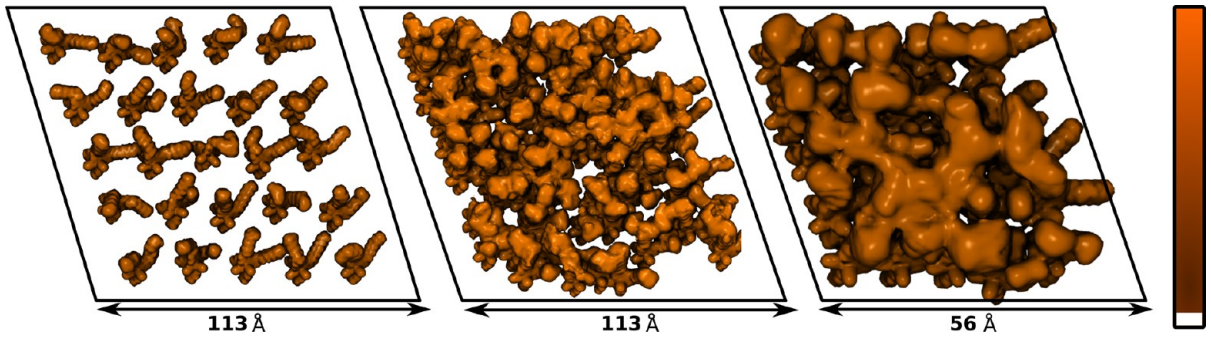


**Figure 6.** Simulated AFM pictures for different mass coverage, (left to right) 33, 66, and 100%. Map of the weighted atomic density of dye molecules. The map is done by replacing each dye atom with a normalized Gaussian distribution of width (standard deviation) equal to the atomic radius. The Gaussian distribution for each atom is then weighted with the occupancy. The various Gaussians are added and distributed on a grid (orange color). The isosurface value is 0.01. The same map with restriction to the parts of dye molecules that are 13−25 Å away from the $TiO_2$ surface is shown in the Supporting Information, Figure S7.

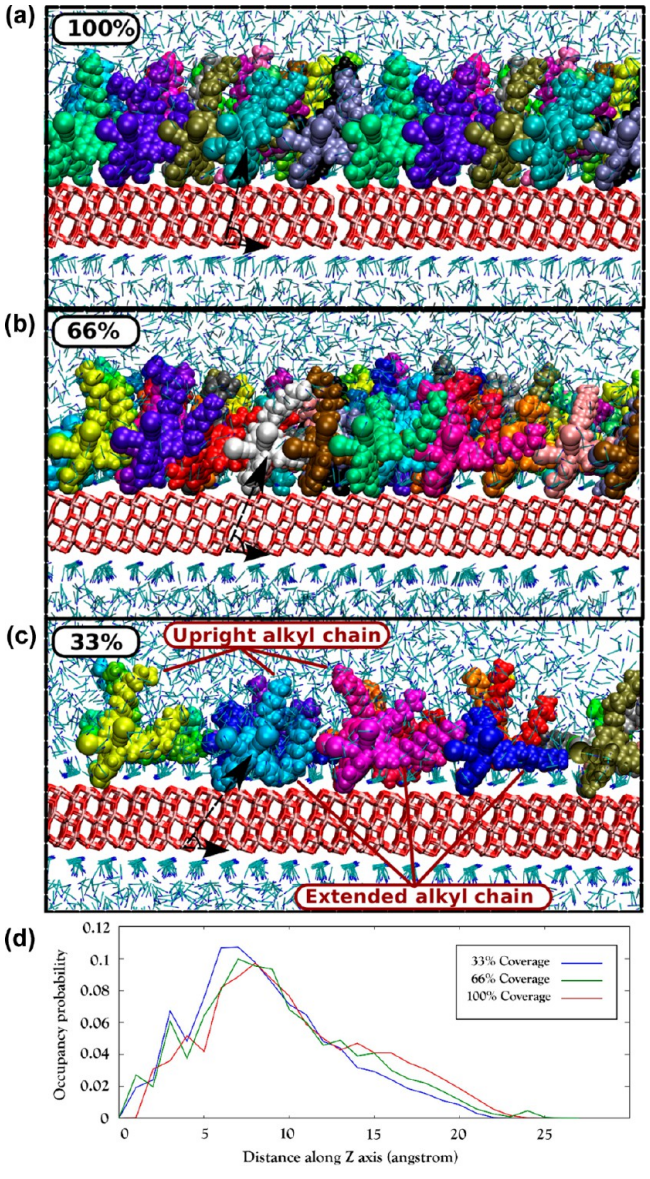


**Figure 7.** (a−c) Side views of the three systems with different mass coverage. The tilting angle is indicated with black arrows. When going to higher mass coverage, more alkyl chains assume an upright position. (d) The probability of finding dye atoms along the *z* axis (normal to the surface) for 20 ns of MD simulation in NVE ensemble.

instantaneous tilting angles shown in the figure for one snapshot are not necessarily identical to the average values).

As the experimental results in this AFM study and in other STM studies[37] suggest, the $TiO_2$ surface templates the dye arrangement via the binding site, and the packing is less driven by dye−dye interactions. Simulations results for the low coverage system (less dye−dye interactions) also show significant energy differences between different dye arrangements on the $TiO_2$ template (Table 1). AFM nanographs at 60% mass coverage suggest the possible coexistence of distinct domains of dye molecules with the alkyl chains either pointing away from the surface, or stretched out along the surface. Indeed our MD simulations results also reflect the coexistence of quasi parallel and quasi vertical alkyl chains and also show that the relative population of the two alkyl chain orientations is density dependent (Figure 7). At low coverage, one alkyl chain is mostly parallel and one is vertical, while at high coverage both alkyl chains are found in a quasi vertical configuration. The intermediate coverage consists of a mixture of dye molecules with these two main configurations. For this intermediate coverage range, we also explored few inhomogeneous configurations with dye domain formation (Supporting Information, Figure S3).

In addition, we analyzed the solvent accessibility of the SAM (Supporting Information, Figure S4). For all three coverages, the dye molecules reduce the accessibility of the solvent to $TiO_2$ with respect to a dye-free surface (Supporting Information, Figure S4, left side). This solvent screening sets in at farther distances and is more effective for higher coverage, where alkyl chains are positioned more vertically and the monolayer thickness is larger.

Besides the conformational change of the alkyl chains with respect to the surface, MD simulations at nominal 100% dye coverage also indicate that the binding location of the molecules close to maximum coverage can be altered. In the areas with densely packed arrangements, dyes encumber each other, forcing their neighbors to take positions that are not usually energetically preferred (in terms of adsorption sites) and can even detach from the surface at higher temperatures (Supporting Information, Figure S5).

## 4. DISCUSSION

Results from AFM measurements and MD computations both indicate that the amphiphilic Z907 dye covers most of the $TiO_2$ surface already at 33% mass coverage by stretching out its alkyl


DOI: 10.1021/acsami.5b01638
ACS Appl. Mater. Interfaces 2015, 7, 10834−10842

chains along the $TiO_2$ surface. For 100% weight coverage, experiment and simulation show that the molecules form a densely packed monolayer, with both alkyl chains adapting an upright conformation. This microscopic observation confirms the common understanding that alkyl chains can shield the $TiO_2$ surface in applications like dye-sensitized solar cells, and it elucidates the way in which they do.

Our observation of two different types of conformation of the dye molecules matches well with previous findings on anisotropic dye molecules by combined NEXAFS and PES studies;[16,43] our measurement offers an independent confirmation by a direct and complementary AFM observation in a relevant liquid environment. The existence of two adsorbed conformations is reminiscent of the well-known "flat lying" and "standing" molecular configurations of alkanethiols SAMs on gold.[44] The analogy with the present case is nonetheless not obvious, given the important differences in the type of bond formed between the dye and the substrate.

Our measurements also provide high-resolution lateral information (i.e., conformity and homogeneity of the film at high mass coverage). Considering the amphiphilic nature of the Z907 molecule, these findings could remain valid for surfactant adsorption at low concentration in general.

In the particular case of dye-sensitized solar cells, the staining of mesoporous $TiO_2$ is carried out at high Z907 dye concentration (250 $\mu$M). However, it is known that it takes several hours for the dye to reach the bottom of a mesoporous film, and even longer to fully saturate the dye uptake in the mesoporous film.[45,46] This indicates that during the staining process, all of the different conformations and different degrees of mass coverage are present in part of the mesoporous $TiO_2$ film. This implies that the results derived by QCM-D and AFM on flat model systems provide meaningful insights that are relevant to the mesoporous system. In particular, amphiphilic sensitizers can effectively cover the $TiO_2$ surface already at low mass coverage, so the shielding of the $TiO_2$ from the electrolyte can be effective even if the staining of deeper layers of the mesoporous $TiO_2$ film is incomplete. Practically, this would result in a working device with good fill factor and photovoltage, but the photocurrent would be inferior to a similar device in which 100% dye mass coverage was achieved. On both flat and mesoporous $TiO_2$, we consistently observe monolayers of Z907, not agglomerations.[19] We observed dye agglomerations only upon special sample preparation procedures (e.g., when the rinsing of the sample was omitted). Furthermore, the existence of molecular rows could be observed on both the flat and mesoporous substrates by AFM in EiPS, supporting the generality of our findings in different electrolytes. The observation of two different conformations is in fact further supported by the two-step adsorption kinetics that are often observed in DSCs.[27,47]

In the more general sense, it is very encouraging that the computational method produces good agreement with the results of the AFM study. The MD simulation only used the quantitative input on the number of dye molecules per area, as obtained experimentally from the QCM-D mass coverage. Computations then produced a detailed description of the adsorbed molecular film in liquid environment, which corresponds very well to the experimental data obtained independently by AFM. The AFM study presented here is at the limit of the resolution that can currently be achieved on molecular films in a relevant liquid environment, but the model at the basis of the MD simulation may still describe the behavior of molecular films correctly at a level that is beyond the resolution of current experimental methods.

## 5. CONCLUSION

In this study, we have combined high-resolution AFM, QCM-D, and MD simulations to elucidate the molecular arrangement of the Z907 dye molecules at the surface of $TiO_2$ in a functionally relevant liquid. Our results detail the formation of the dye monolayer, showing several molecular conformations on the surface at different dye concentration.

Future work will address molecular films that consist of functional molecules co-adsorbed with chelating agents such as bile acids (e.g., porphyrin sensitizers and cheno deoxycholic acid), where the nature of interaction and the arrangement of dye and co-adsorbate within the sensitizing film still wait to be unveiled.

## ■ ASSOCIATED CONTENT

### Supporting Information

High-resolution AFM image of the Z907 dye layer in acetonitrile; orientation with respect to the crystal lattice of packing; and calculated solvent density along the $z$ axis (vertical to the $TiO_2$ slab). The Supporting Information is available free of charge on the ACS Publications website at DOI: 10.1021/acsami.5b01638.

## ■ AUTHOR INFORMATION


### Corresponding Author

*E-mail: hauke.harms@alumni.epfl.ch.

### Present Address

[⊥]IBM Research GmbH, Zurich Research Laboratory, 8803 Rueschlikon, Switzerland


### Author Contributions

[#]These authors contributed equally. The manuscript was written through contributions of all authors. All authors have given approval to the final version of the manuscript.


### Funding

K.V. acknowledges funding from the Swiss National Science Foundation through the Ambizione Fellowship (PZ00P2_136941). U.R. acknowledges funding from the Swiss National Science Foundation via individual grant No. 200020-146645, the NCCRs MUST and MARVEL, and support from the Swiss National Computing Center (CSCS) and the CADMOS project for computing resources. M.G. thanks the European Research Council (ERC) for supporting part of this work under the advanced research grant (no. 247404) MESOLIGHT. H.A.H. acknowledges funding from the Swiss National Science Foundation (SNF). M.G. and N.T. acknowledge funding from the King Abdullah University of Science and Technology (KAUST, Award no. KUS-C1-015-21).


### Notes

The authors declare no competing financial interest.

## ■ ACKNOWLEDGMENTS


We thank S. M. Zakeeruddin for providing the Z907 dye and EiPS.


## ■ REFERENCES


(1) Akkerman, H. B.; Blom, P. W. M.; de Leeuw, D. M.; de Boer, B. Towards Molecular Electronics with Large-Area Molecular Junctions. *Nature* **2006**, *441*, 69−72.




DOI: 10.1021/acsami.5b01638
*ACS Appl. Mater. Interfaces* 2015, 7, 10834−10842

(2) Bain, C. D.; Whitesides, G. M. Correlations Between Wettability and Structure in Monolayers of Alkanethiols Adsorbed on Gold. *J. Am. Chem. Soc.* **1988**, *110*, 3665−3666.
(3) Flink, S.; Van Veggel, F.; Reinhoudt, D. N. Sensor Functionalities in Self-Assembled Monolayers. *Adv. Mater.* **2000**, *12*, 1315−1328.
(4) Langer, R.; Tirrell, D. A. Designing Materials for Biology and Medicine. *Nature* **2004**, *428*, 487−492.
(5) O'Regan, B.; Grätzel, M. A Low-Cost, High-Efficiency Solar Cell Based on Dye-Sensitized Colloidal $TiO_2$ Films. *Nature* **1991**, *353*, 737−740.
(6) Love, J. C.; Estroff, L. A.; Kriebel, J. K.; Nuzzo, R. G. Self-Assembled Monolayers of Thiolates on Metals as a Form of Nanotechnology. *Chem. Rev.* **2005**, *105*, 1103−1169.
(7) Hagfeldt, A.; Boschloo, G.; Sun, L.; Kloo, L.; Pettersson, H. Dye-Sensitized Solar Cells. *Chem. Rev.* **2010**, *110*, 6595−6663.
(8) Han, L.; Islam, A.; Chen, H.; Malapaka, C.; Zhang, S.; Yang, X.; Yanagida, M. High-Efficiency Dye-Sensitized Solar Cell with a Novel Co-adsorbent. *Energy Environ. Sci.* **2012**, *5*, 6057−6060.
(9) Gao, F.; Wang, Y.; Shi, D.; Zhang, J.; Wang, M.; Jing, X.; Humphry-Baker, R.; Wang, P.; Zakeeruddin, S. M.; Grätzel, M. Enhance the Optical Absorptivity of Nanocrystalline $TiO_2$ Film with High Molar Extinction Coefficient Ruthenium Sensitizers for High Performance Dye-Sensitized Solar Cells. *J. Am. Chem. Soc.* **2008**, *130*, 10720−10728.
(10) Grätzel, M. The Advent of Mesoscopic Injection Solar Cells. *Prog. Photovoltaics: Res. Appl.* **2006**, *14*, 429−442.
(11) Yella, A.; Lee, H. W.; Tsao, H. N.; Yi, C.; Chandiran, A. K.; Nazeeruddin, M. K.; Diau, E. W. G.; Yeh, C. Y.; Zakeeruddin, S. M.; Grätzel, M. Porphyrin-Sensitized Solar Cells with Cobalt (II/III)-Based Redox Electrolyte Exceed 12% Efficiency. *Science* **2011**, *334*, 629−634.
(12) Kuna, J. J.; Voïtchovsky, K.; Singh, C.; Jiang, H.; Mwenifumbo, S.; Ghorai, P. K.; Stevens, M. M.; Glotzer, S. C.; Stellacci, F. The Effect of Nanometre-Scale Structure on Interfacial Energy. *Nat. Mater.* **2009**, *8*, 837−842.
(13) Schiffmann, F.; VandeVondele, J.; Hutter, J.; Wirz, R.; Urakawa, A.; Baiker, A. Protonation-Dependent Binding of Ruthenium Bipyridyl Complexes to the Anatase(101) Surface. *J. Phys. Chem. C* **2010**, *114*, 8398−8404.
(14) Yu, S.; Ahmadi, S.; Zuleta, M.; Tian, H.; Schulte, K.; Pietzsch, A.; Hennies, F.; Weissenrieder, J.; Yang, X.; Göthelid, M. Adsorption Geometry, Molecular Interaction, and Charge Transfer of Triphenylamine-based Dye on Rutile $TiO_2$(110). *J. Chem. Phys.* **2010**, *133*, 224704.
(15) Marinado, T.; Hahlin, M.; Jiang, X.; Quintana, M.; Johansson, E. M. J.; Gabrielsson, E.; Plogmaker, S.; Hagberg, D. P.; Boschloo, G.; Zakeeruddin, S. M.; Grätzel, M.; Siegbahn, H.; Sun, L.; Hagfeldt, A.; Rensmo, H. Surface Molecular Quantification and Photoelectrochemical Characterization of Mixed Organic Dye and Coadsorbent Layers on $TiO_2$ for Dye-Sensitized Solar Cells. *J. Phys. Chem. C* **2010**, *114*, 11903−11910.
(16) Rienzo, A.; Mayor, L. C.; Magnano, G.; Satterley, C. J.; Ataman, E.; Schnadt, J.; Schulte, K.; O'Shea, J. N. X-Ray Absorption and Photoemission Spectroscopy of Zinc Protoporphyrin Adsorbed on Rutile $TiO_2$(110) Prepared by in Situ Electrospray Deposition. *J. Chem. Phys.* **2010**, *132*, 084703.
(17) Kley, C. S.; Dette, C.; Rinke, G.; Cechal, J.; Jung, S. J.; Baur, M.; Dürr, M.; Rauschenbach, S.; Giustino, F.; Stepanow, S.; Kern, K. Atomic-Scale Observation of Multiconformational Binding and Energy Level Alignment of Ruthenium-Based Photosensitizers on $TiO_2$ Anatase. *Nano Lett.* **2014**, *14*, 563−569.
(18) Sasahara, A.; Fujio, K.; Koide, N.; Han, L.; Onishi, H. STM Imaging of a Model Surface of Ru(4,4′-Dicarboxy-2,2′-bipyridine)$_2$(NCS)$_2$ Dye-Sensitized $TiO_2$ Photoelectrodes. *Surf. Sci.* **2010**, *604*, 106−110.
(19) Marquet, P.; Andersson, G.; Snedden, A.; Kloo, L.; Atkin, R. Molecular Scale Characterization of the Titania−Dye−Solvent Interface in Dye-Sensitized Solar Cells. *Langmuir* **2010**, *26*, 9612−9616.
(20) Fukuma, T.; Higgins, M. J.; Jarvis, S. P. Direct Imaging of Lipid−Ion Network Formation Under Physiological Conditions by Frequency Modulation Atomic Force Microscopy. *Phys. Rev. Lett.* **2007**, *98*, 106101.
(21) Fukuma, T.; Ueda, Y.; Yoshioka, S.; Asakawa, H. Atomic-Scale Distribution of Water Molecules at the Mica−Water Interface Visualized by Three-Dimensional Scanning Force Microscopy. *Phys. Rev. Lett.* **2010**, *104*, 016101.
(22) Voïtchovsky, K.; Kuna, J. J.; Contera, S. A.; Tosatti, E.; Stellacci, F. Direct Mapping of the Solid−Liquid Adhesion Energy with Subnanometre Resolution. *Nat. Nanotechnol.* **2010**, *5*, 401−405.
(23) Zakeeruddin, S. M.; Nazeeruddin, M. K.; Humphry-Baker, R.; Pechy, P.; Quagliotto, P.; Barolo, C.; Viscardi, G.; Grätzel, M. Design, Synthesis, and Application of Amphiphilic Ruthenium Polypyridyl Photosensitizers in Solar Cells Based on Nanocrystalline $TiO_2$ Films. *Langmuir* **2002**, *18*, 952−954.
(24) Wang, P.; Zakeeruddin, S. M.; Moser, J. E.; Nazeeruddin, M. K.; Sekiguchi, T.; Grätzel, M. A Stable Quasi-Solid-State Dye-Sensitized Solar Cell with an Amphiphilic Ruthenium Sensitizer and Polymer Gel Electrolyte. *Nat. Mater.* **2003**, *2*, 402−407.
(25) Rodahl, M.; Hook, F.; Krozer, A.; Brzezinski, P.; Kasemo, B. Quartz Crystal Microbalance Setup for Frequency and Q-Factor Measurements in Gaseous and Liquid Environments. *Rev. Sci. Instrum.* **1995**, *66*, 3924−3930.
(26) Rodahl, M.; Kasemo, B. Frequency and Dissipation-Factor Responses to Localized Liquid Deposits on a QCM Electrode. *Sens. Actuators, B* **1996**, *37*, 111−116.
(27) Harms, H. A.; Tétreault, N.; Gusak, V.; Kasemo, B.; Grätzel, M. In-Situ Investigation of Dye Adsorption on $TiO_2$ Films Using a Quartz Crystal Microbalance with Dissipation Technique. *Phys. Chem. Chem. Phys.* **2012**, 9037−9040.
(28) Voïtchovsky, K. Anharmonicity, Solvation Forces, And Resolution in Atomic Force Microscopy at the Solid−Liquid Interface. *Phys. Rev. E* **2013**, *88*, 022407.
(29) Cornell, W. D.; Cieplak, P.; Bayly, C. I.; Gould, I. R.; Merz, K. M.; Ferguson, D. M.; Spellmeyer, D. C.; Fox, T.; Caldwell, J. W.; Kollman, P. A. A Second Generation Force Field for the Simulation of Proteins, Nucleic Acids, and Organic Molecules. *J. Am. Chem. Soc.* **1995**, *117*, 5179−5197.
(30) Bandura, A. V.; Kubicki, J. D. Derivation of Force Field Parameters for $TiO_2$−$H_2O$ Systems From Ab Initio Calculations. *J. Phys. Chem. B* **2003**, *107*, 11072−11081.
(31) Case, D. A.; Darden, T. A.; Cheatham, T. E., III; Simmerling, C. L. AMBER 12—Amber Package. University of California 2012.
(32) Bayly, C. I.; Cieplak, P.; Cornell, W.; Kollman, P. A. A Well-Behaved Electrostatic Potential Based Method Using Charge Restraints for Deriving Atomic Charges: The RESP Model. *J. Phys. Chem.* **1993**, *97*, 10269−10280.
(33) Frisch, M. J.; Trucks, G. W.; Schlegel, H. B.; Scuseria, G. E.; Robb, M. A.; Cheeseman, J. R.; Scalmani, G. Gaussian 09, revision A. 1. Gaussian Inc.: Wallingford, CT, 2009.
(34) Sushko, M. L.; Gal, A. Y.; Shluger, A. L. Interaction of Organic Molecules with the $TiO_2$ (110) Surface: Ab Inito Calculations and Classical Force Fields. *J. Phys. Chem. B* **2006**, *110*, 4853−4862.
(35) Jorgensen, W. L.; Tirado-Rives, J. The OPLS [Optimized Potentials for Liquid Simulations] Potential Functions for Proteins, Energy Minimizations for Crystals of Cyclic Peptides and Crambin. *J. Am. Chem. Soc.* **1988**, *110*, 1657−1666.
(36) Pastore, M.; Angelis, F. D. First-Principles Computational Modeling of Fluorescence Resonance Energy Transfer in Co-Sensitized Dye Solar Cells. *J. Phys. Chem. Lett.* **2012**, *3*, 2146−2153.
(37) Grinter, D. C.; Nicotra, M.; Thornton, G. Acetic Acid Adsorption on Anatase $TiO_2$ (101). *J. Phys. Chem. C* **2012**, *116*, 11643−11651.
(38) Polander, L. E.; Yella, A.; Curchod, B. F. E.; Ashari Astani, N.; Teuscher, J.; Scopelliti, R.; Gao, P.; Mathew, S.; Moser, J. E.; Tavernelli, I.; Rothlisberger, U.; Grätzel, M.; Nazeeruddin, M. K.; Frey, J. Towards Compatibility Between Ruthenium Sensitizers and Cobalt


DOI: 10.1021/acsami.5b01638
*ACS Appl. Mater. Interfaces* 2015, 7, 10834−10842

Electrolytes in Dye-Sensitized Solar Cells. *Angew. Chem., Int. Ed.* **2013**, *52*, 8731−8735.
(39) Discovery Studio Modeling Environment, release 4.0; Accelrys Software, Inc.: San Diego, 2013.
(40) Tétreault, N.; Heiniger, L.-P.; Stefik, M.; Labouchère, P. L.; Arsenault, É.; Nazeeruddin, N. K.; Ozin, G. A.; Grätzel, M. Atomic Layer Deposition for Novel Dye-Sensitized Solar Cells. *ECS Trans.* **2011**, *41*, 303−314.
(41) Yanada, K.; Chiba, K.; Yamaguchi, Y.; Yamamoto, H. Characteristics of Dye-Sensitized Solar Cells Using Linear Sulfones as an Electrolyte Solvent. *Electrochim. Acta* **2012**, *79*, 163−167.
(42) Chiba, K.; Ueda, T.; Yamaguchi, Y.; Oki, Y.; Saiki, F.; Naoi, K. Electrolyte Systems for High Withstand Voltage and Durability II. Alkylated Cyclic Carbonates for Electric Double-Layer Capacitors. *J. Electrochem. Soc.* **2011**, *158*, A1320.
(43) Hahlin, M.; Johansson, E. M. J.; Plogmaker, S.; Odelius, M.; Hagberg, D. P.; Sun, L.; Siegbahn, H.; Rensmo, H. Electronic and Molecular Structures of Organic Dye/$TiO_2$ Interfaces for Solar Cell Applications: A Core Level Photoelectron Spectroscopy Study. *Phys. Chem. Chem. Phys.* **2010**, *12*, 1507.
(44) Schwartz, D. K. Mechanisms and Kinetics of Self-Assembled Monolayer Formation. *Annu. Rev. Phys. Chem.* **2001**, *52*, 107−137.
(45) O'Regan, B.; Xiaoe, L.; Ghaddar, T. Dye Adsorption, Desorption, and Distribution in Mesoporous $TiO_2$ Films, and Its Effects on Recombination Losses in Dye Sensitized Solar Cells. *Energy Environ. Sci.* **2012**, *5*, 7203−7215.
(46) Gusak, V.; Heiniger, L.-P.; Graetzel, M.; Langhammer, C.; Kasemo, B. Time-Resolved Indirect Nanoplasmonic Sensing Spectroscopy of Dye Molecule Interactions with Dense and Mesoporous $TiO_2$ Films. *Nano Lett.* **2012**, *12*, 2397−2403.
(47) Gusak, V.; Nkurunziza, E.; Langhammer, C.; Kasemo, B. Real-Time Adsorption and Desorption Kinetics of Dye Z907 on a Flat Mimic of Dye-Sensitized Solar Cell $TiO_2$ Photoelectrodes. *J. Phys. Chem. C* **2014**, *118*, 17116−17122.


DOI: 10.1021/acsami.5b01638
*ACS Appl. Mater. Interfaces* 2015, 7, 10834−10842